Antarct. Meteorite Res., **10**, 355–372, 1997

PETROLOGY AND CHEMISTRY OF THE MILES IIE IRON. I: DESCRIPTION AND PETROLOGY OF TWENTY NEW SILICATE INCLUSIONS

Yukio IKEDA[1], Mitsuru EBIHARA[2] and Martin PRINZ[3]

[1]*Department of Earth Sciences, Ibaraki University, Mito 310*
[2]*Department of Chemistry, Tokyo Metropolitan University, Hachioji-shi, Tokyo 192–03*
[3]*Department of Earth and Planetary Sciences, American Museum of Natural History, New York, NY 10024, U. S. A.*

Abstract: A petrologic study of twenty new silicate inclusions (15 gabbroic, 5 cryptocrystalline) in the Miles IIE iron was undertaken in order to help clarify the petrogenesis of this meteorite and its relationship to other IIE irons with silicates, as well as H-group chondrites. Nine of the inclusions were analyzed by the INAA method, which is presented in a companion paper. The results indicate that Miles was formed by shock events on an H-group chondrite parent body. It formed silicate melt and Fe-Ni-S-P melt by about 25% partially melting, and left behind olivine-orthopyroxene residues. The silicate melt was a crystal mush which consisted of phenocrysts of high-Ca pyroxene, orthopyroxene and plagioclase, and residual melt. The phenocryst-enriched mush formed irregular-shaped gabbroic inclusions, which also contain minor olivine, inverted pigeonite, antiperthite, K-feldspar, tridymite, glass, chromite, rutile, ilmenite, armalcolite, chlorapatite, whitlockite, kamacite, taenite, schreibersite, troilite and pentlandite. The residual melt formed round- to ellipsoidal-shaped cryptocrystalline inclusions, which contain microphenocrysts of alkali feldspar or phenocrysts of pyroxene. The crystal mush was mixed with abundant Fe-Ni-S-P melt, from which most of the sulfur escaped, and from which some of the phosphorus reacted with the silicate melts, resulting in their reduction. This reduction produced Ca-poor magnesian orthopyroxene and Ca-poor plagioclase in the gabbroic inclusions. The degree of reduction was, however, more intense in the cryptocrystalline inclusions than in the gabbroic inclusions. The remaining phosphorus in the solid host metal exsolved as schreibersite around the silicate inclusions.

1. Introduction

The Miles IIE iron contains many silicate inclusions, and twenty-nine of them were petrologically studied in detail by IKEDA and PRINZ (1996), using six thin sections. However, the trace element compositions of the Miles silicate inclusions were not yet analyzed. Therefore, we carried out a petrologic study of twenty new silicate inclusions from two Miles slabs, and separated nine of them for instrumental neutron activation analyses (INAA). In this paper we present the petrography and petrology of the twenty new silicate inclusions, and a companion paper (EBIHARA *et al.*, 1997) gives the trace element chemistry of nine of them and the host iron.

Silicate inclusions in IIE irons have oxygen isotopic compositions similar to those of H-group chondrites (CLAYTON and MAYEDA, 1983; RUBIN *et al.*, 1986), indicating that they may have an intimate genetic relationship. However, the origin of IIE irons is controversial, and some models have been presented: a silicate melt was trapped in a solidifying iron mass (WASSERBURG *et al.*, 1968), metal has been mixed with the silicates during a shock event (PRINZ *et al.*, 1983), IIE irons formed as pools of impact-produced melt near the base of a thick megaregolith (WASSON and WANG, 1986), IIE irons were produced through early mixing and differentiation in a core-mantle environment of the IIE parent body (MCCOY, 1995), and Fe-Ni-S melt and silicate melts were produced by batch or partial melting of H-group chondrites and mixed with each other to form IIE irons near the surface of an H-group chondrite parent body (IKEDA and PRINZ, 1996). This paper, and the companion paper, discuss the petrology and chemistry of the Miles silicate inclusions and host metal in order to help clarify the petrogenesis of the group.

2. Analytical Methods

The chemical compositions of the constituent minerals were obtained with a JEOL 733 electron-probe micro-analyzer (EPMA at the Department of Earth Sciences, Ibaraki Univ.). An accelerating voltage of 15 kV and a probe current of 3–5 nA were used. The compositions were corrected by the BENCE and ALBEE (1968) method for silicates, oxides, and phosphates, and by the standard ZAF method for metal and sulfides.

3. Description and Mineralogy of Silicate Inclusions and the Metal Host

3.1. Slicate inclusions

The silicate inclusions in Miles are 2–10 mm in size and make up about 10–20% by volume (IKEDA and PRINZ, 1996). In this paper, we studied twenty new inclusions from two large slabs (AMNH 4866-1 and 4866-2), and these were numbered as shown in Table 1. IKEDA and PRINZ (1996) studied twenty-nine silicate inclusions and showed that they can be classified into two textural types, gabbroic and cryptocrystalline. The textural types of the inclusions studied here are the same and their constituent minerals are summarized in Table 1. Representative compositions of the minerals in these inclusions are shown in Tables 2 and 3.

Of the silicate inclusions studied here and in IKEDA and PRINZ (1996), 42 inclusions are gabbroic and 7 are cryptocrystalline. In general, the gabbroic inclusions have irregular outlines, whereas the cryptocrystalline inclusions have rounded or ellipsoidal outlines. The silicate inclusions are partly surrounded by schreibersite. The gabbroic inclusions are holocrystalline, except for the rare occurrence of glass with rhyolitic composition, and the cryptocrystalline inclusions have cryptocrystalline groundmasses.

3.2. Gabbroic inclusions

The gabbroic inclusions are coarse-grained, up to 5 mm, and consist mainly of

Table 1. Textures (gabbroic or cryptocrystalline) and mineral assemblages of the Miles silicate inclusions studied.

Inclusion	Texture	Ol	Cpx	Ipig	Opx	Pl	Ant-P	Kf	Tridy	Rh-Gl	Cry-Ab	Chm	Rut	Aml	Ilm	Wht	Apt	Comments (see text)
1A	Cryptocry.							+			++		+					Ca-free Fd
*1B	Gabbroic		++		++	+		+	+			+	+			+		Magnesian Opx
*1C	〃	+	++		++	++		+				+	+		+	+	+	Opx-Wht aggregate
*1D	〃		+		+	++	+	+										
*1E	Cryptocry.				+		+				++	+	+			+		Opx needles, Al-Chm
*1F	Gabbroic		++	+	++	+	+	+	+			+		+				
*1G	Cryptocry.		+		++		+				++	+				+	+	A large Pyx pheno.
*1H	〃		+		+						++	+				+	+	Wht needles, Ca-free Fd
*1I	Gabbroic	+	++		++	+		+	+			++	+		+	+	+	Symplec., Rut-Ilm ex.
*1J	〃		+		+	++	+	+	+			+					+	
2A	Gabbroic		+		++	++		+	+	+		+	+		+	+	+	
2B	〃		++		+	++			+			+					+	
2C	〃		+			++	+	+	+									
2D	〃		++		+	++		+										
2E	Cryptocry.							+			++							Tridy-Ab aggregate
2F	Gabbroic					++												Ca-free Fd
2G	〃		+		+	++		+							+		+	
2H	〃		++	+	+	++	+	+	+									
2I	〃	+	++		++	++						+	+		+	+		
2J	〃		++		++	++		+								+	+	

In addition to the minerals listed here, small but variable amounts of kamacite, taenite, schreibersite, and sulfides occur in these inclusions, although kamacites have often been altered to limonite. Inclusions with the symbol * were analyzed by the INAA method. ++:major, +:minor. Abbreviations: Ol (olivine), Cpx (high-Ca pyroxene), IPig (inverted pigeonite), Opx (orthopyroxene), Pl (Plagioclase), Ant-P (antiperthite, or anorthoclase), Kf (K-feldspar), Tridy (tridymite), Rh-Gl (rhyolitic glass), Cry-Ab (cryptocrystalline albite), Chm (chromite), Rut (rutile), Aml (armalcolite), Ilm (ilmenite), Wht (whitlockite), Apt (Cl-apatite). Ca-free Fd in comments means Ca-free cryptocrystalline albite and Ca-free K-feldspar.

high-Ca clinopyroxene, orthopyroxene, and plagioclase (Fig. 1-1). Minor amounts of olivine, inverted pigeonite, anti-perthite, K-feldspar, tridymite, glass, chromite, rutile, ilmenite, armalcolite, chlorapatite, whitlockite, kamacite, taenite, schreibersite, troilite, and pentlandite are also present. Plagioclase is the most abundant phase (about 47 vol%; IKEDA and PRINZ, 1996), the second is high-Ca pyroxene (34 vol%), and the third is orthopyroxene (17 vol%), although modal ratios of the three main phases differ considerably among the gabbroic inclusions.

Olivine occurs in three inclusions of the 42 gabbroic ones studied and is always wholly or partly included in large orthopyroxenes, and has a corroded outline (Fig. 1-2). The olivine compositions differ slightly among the gabbroic inclusions and their MgO/(MgO+FeO) molecular ratios (hereafter, mg ratios) range from 0.85 to 0.90 (Fig. 2). Olivine (Fo_{86-89}) in inclusion 1C coexists with magnesian orthopyroxene (En_{84-88} $Wo_{1-1.5}$), chromite, rutile, ilmenite, kamacite, taenite, whitlockite, and an intergrowth of magnesian orthopyroxene and whitlockite (Fig. 1-3). This intergrowth includes small metallic grains and seems to have replaced olivine (Fig. 1-3, 1-4). Olivine (Fo_{88-90}) in inclusion 1I is included in a large orthopyroxene ($En_{76-83}Wo_{1-4}$) (Fig. 1-5), with a reac-

Table 2. Representative compositions of minerals in Miles gabbroic inclusions.

Inclusion	2I	1C	1C	2I	1C	1B	1C	1C
	Ol	Ol	mOpx	mOpx	Opx	Cpx	Cpx	Pl
SiO_2	39.53	40.14	56.31	56.46	55.60	53.47	53.10	65.67
TiO_2	0.00	0.00	0.24	0.34	0.29	1.87	0.69	0.02
Al_2O_3	0.00	0.00	0.15	0.13	0.21	0.32	0.58	19.96
Cr_2O_3	0.00	0.00	0.11	0.17	0.37	2.23	1.61	0.00
FeO	14.44	12.01	8.83	9.64	13.19	6.05	6.22	0.16
MnO	0.56	0.60	0.66	0.63	0.80	0.43	0.43	0.07
MgO	45.17	46.37	32.60	32.24	27.09	14.94	15.53	0.00
CaO	0.01	0.04	0.52	0.69	1.88	18.99	20.19	1.54
Na_2O	0.00	0.00	0.00	0.00	0.12	1.61	1.08	11.01
K_2O	0.00	0.00	0.00	0.00	0.00	0.00	0.00	0.37
ZnO								
ZrO_2								
Total	99.71	99.16	99.43	100.32	99.55	99.92	99.43	98.82

	1B	1B	2A	1C	1C	2I	1C	1F
	Pl	Kf	Glass	Chm	Ilm	Ilm	Rut	Aml
SiO_2	68.24	64.46	76.65	0.00	0.00	0.00	0.00	0.13
TiO_2	0.00	0.03	0.15	3.33	57.50	53.60	99.34	68.05
Al_2O_3	19.23	17.79	14.69	3.98	0.00	0.00	0.03	0.27
Cr_2O_3	0.00	0.00	0.03	60.98	0.06	0.00	0.00	13.57
FeO	0.41	0.44	0.66	21.47	29.86	40.49	0.50	7.87
MnO	0.04	0.00	0.00	1.11	1.49	0.77	0.00	0.63
MgO	0.00	0.00	0.00	6.51	11.13	4.79	0.01	1.98
CaO	0.42	0.06	0.11	0.00	0.00	0.00	0.06	2.38
Na_2O	11.40	1.05	2.32	0.00	0.00	0.00	0.07	0.72
K_2O	0.47	15.11	4.46	0.00	0.00	0.00	0.01	0.02
ZnO				1.78				
ZrO_2								3.10
Total	100.22	98.94	99.07	99.17	100.05	99.65	100.01	98.72

Abbreviations: Ol (olivine), mOpx (magnesian orthopyroxene), Opx (orthopyroxene), Cpx (high-Ca clinopyroxene), Pl (plagioclase), Kf (potassium feldspar), Glass (glass with rhyolitic composition), Chm (chromite), Ilm (ilmenite), Rut (rutile), and Aml (armalcolite).

tion zone between the olivine grains and the orthopyroxene host. The reaction zone is 0–100 μm in width, and consists mainly of magnesian orthopyroxene ($En_{85\text{-}88}$ Wo_1), whitlockite, chromite, metal, and symplectic intergrowths of chromite and magnesian orthopyroxene (Fig. 1-6).

Pyroxene in the gabbroic inclusions occurs as large phenocrysts, and high-Ca pyroxene phenocrysts often include smaller orthopyroxenes, or vice versa (Fig. 1-1). The larger high-Ca pyroxenes often show exsolution textures in their cores (Fig. 1-7), but the smaller grains do not (Fig. 1-9). The compositions of the high-Ca pyroxenes plot within a small range in Fig. 2, but their minor element contents, such as Al_2O_3, exhibit zoning; Al_2O_3 contents of high-Ca pyroxene are high in the cores and decrease towards the rims (IKEDA and PRINZ, 1996). Inverted pigeonite is rarely included in

Table 3. Representative compositions of minerals in Miles cryptocrystalline inclusions.

Inclusions	1A	1E	2E	1E	1E	1E	1E	2E	1E	1E
	Cryptocrystalline Ab			n.Opx	n.Opx	Microphen.Fd		Kf	Chm	Chm
SiO_2	67.55	71.03	69.40	54.46	55.67	70.86	68.54	67.92	0.00	0.00
TiO_2	0.05	0.24	0.44	0.39	0.39	0.27	0.17	0.19	0.11	0.44
Al_2O_3	18.79	18.30	18.13	1.77	2.16	18.26	18.27	17.27	29.48	23.80
Cr_2O_3	0.00	0.00	0.00	0.37	0.81	0.00	0.00	0.04	39.77	44.77
FeO	1.13	0.00	0.06	8.45	8.88	0.14	0.00	0.46	13.16	14.50
MnO	0.00	0.00	0.00	0.88	1.04	0.00	0.00	0.05	1.28	1.73
MgO	0.00	0.00	0.19	32.86	29.52	0.00	0.00	0.07	11.16	9.97
CaO	0.00	0.57	0.00	0.42	0.74	0.84	0.73	0.00	0.00	0.00
Na_2O	11.74	9.96	10.91	0.03	0.06	9.43	6.25	1.32	0.00	0.04
K_2O	0.27	0.02	0.36	0.00	0.00	0.67	5.76	12.50	0.00	0.00
ZnO									4.12	3.90
Total	99.53	100.13	99.48	99.63	99.26	100.46	99.72	99.82	99.07	99.16

Abbreviations; Ab (albite), n.Opx (needle crystals of orthopyroxene), Microphen.Fd (microphenocrystic alkali feldspar), Kf (K-feldspar), and Chm (chromite).

large high-Ca pyroxene or orthopyroxene phenocrysts (Fig. 1-7).

Orthopyroxene in the gabbroic inclusions have normal chemical zoning in the cores and reverse zoning in the rims; the cores are richer in Al_2O_3 than the rims (IKEDA and PRINZ, 1996). The composite zoning of orthopyroxene phenocryste, reported by IKEDA and PRINZ (1996), is shown in Fig. 3 by dashed lines. Phenocrystic orthopyroxene in the gabbroic inclusions has mg ratios from 0.74 to 0.83, with Wo contents from 1 to 4% (Fig. 2), and their Al_2O_3 contents are consistent with the compositional trend shown by the dashed lines in Fig. 3. In addition to the phenocrystic orthopyroxene, more magnesian orthopyroxene occurs in close association with olivine in some gabbroic inclusions. They have mg ratios from 0.83 to 0.88, with Wo contents of 0.5 to 1.5% (Fig. 2). They plot as an extension of the reversely zoned orthopyroxene, as shown in Fig. 3.

Large plagioclase grains show normal zoning from An-rich cores (An_{10-15}) to An-poor rims (An_{1-5}) (IKEDA and PRINZ, 1996), and they probably were phenocrysts. Small plagioclase grains have sodic compositions which are similar to that of the rims of large plagioclase grains. The compositions of most plagioclases in the gabbroic inclusions are An_{1-10}, with Or contents from 1 to 5% (Fig. 4).

K-feldspar occurs as euhedral grains (Fig. 1-8) and is intimately associated with intergrowths of anti-perthite and tridymite (Fig. 1-8). K-feldspar is Or_{87-93}, with An_{0-1} (Fig. 4). Rarely, intergrowths of albite and tridymite are observed in interstitial spaces between high-Ca pyroxene or orthopyroxene grains (Fig. 1-9). Glass occurs rarely in some gabbroic inclusions, with or without tridymite (Fig. 1-10), and has rhyolitic compositions, as shown in Table 2.

Chromite is a common mineral in the gabbroic inclusions and sometimes occurs as phenocrystic large grains. The compositions of chromites differ among the gabbroic inclusions, but most are rich in Cr (Fig. 5). The ZnO contents range from 0.3–2.0 wt% (IKEDA and PRINZ, 1996; this study). A large phenocrystic chromite in gabbroic inclusion 1I (Fig. 1-5) includes needles of rutile and ilmenite in its core (Fig. 1-11);

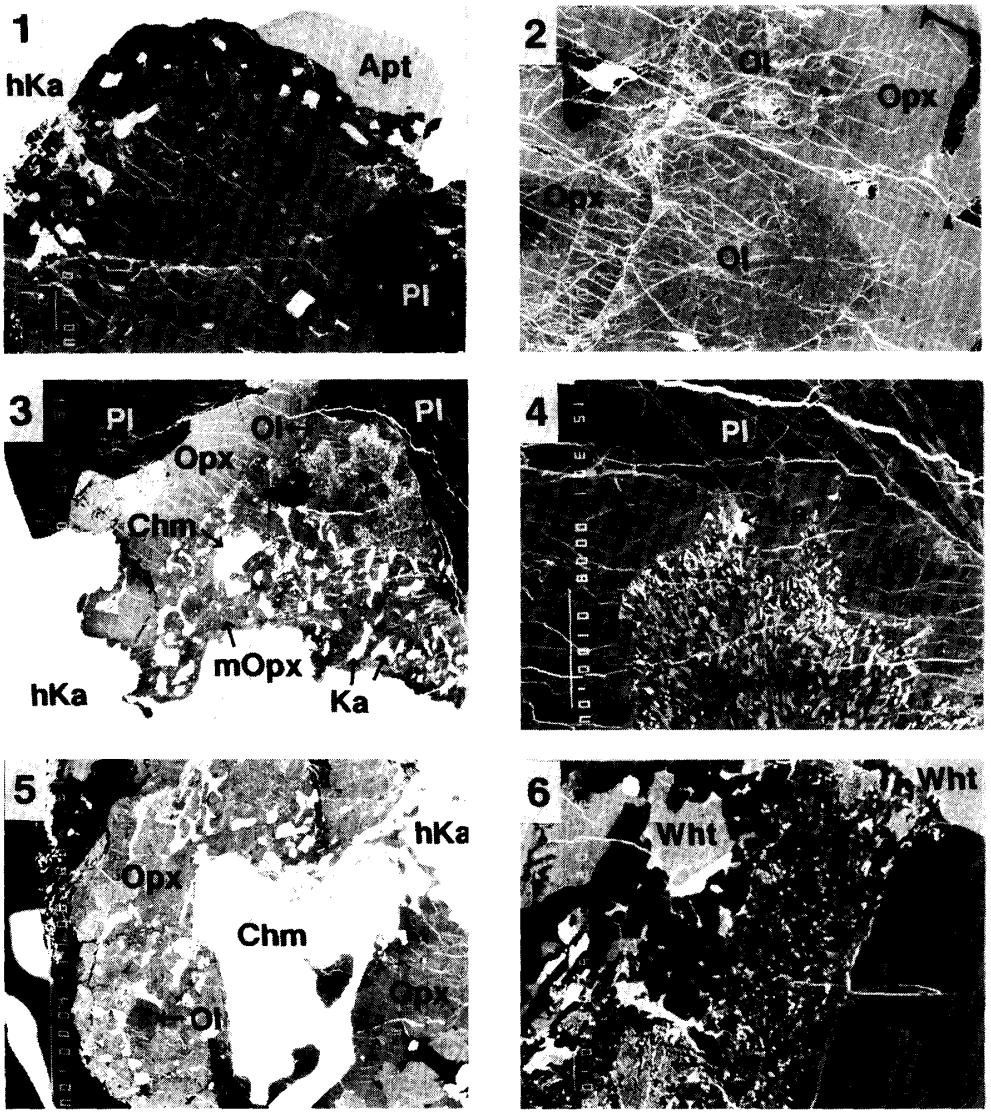

Fig. 1. Back-scattered-electron (BSE) images of Miles gabbroic inclusions from 1-1 to 1-12, cryptocrystalline inclusions from 1-13 to 1-18, and host metal from 1-19 to 1-20. Abbreviation: Ol (olivine), Cpx (high-Ca clinopyroxene), Opx (orthopyroxene), Pl (plagioclase), Af (alkali feldspar), Kf (K-feldspar), Tridy (tridymite), Gl (glass with rhyolitic composition), Cry-Ab (cryptocrystalline albite), Chm (chromite), Rut (rutile), Aml (armalcolite), Ilm (ilmenite), Whl (whitlockite), Apt (Cl-apatite), Ka (kamacite in silicate inclusions), hKa (kamacite as host metal), and Ta (taenite).

Fig. 1-1. Large clinopyroxene grains are phenocrysts, including small orthopyroxene grains. Plagioclase occurs as large grains, filling interstitial spaces between pyroxene phenocrysts. Apatite is often observed at boundaries between silicate inclusions and the host metal, and tridymite sometimes occurs in inclusion rims. Gabbroic inclusion 1I. Width is about 1180 μm.

Fig. 1-2. Relic olivine is sometimes included in large orthopyroxene grains, and shows a corroded outline. Gabbroic inclusion 2I. Width is about 1180 μm.

Fig. 1-3. An aggregate of olivine, magnesian orthopyroxene (mOpx), whitlockite, kamacite, and chromite with a small amount of taenite, rutile, and ilmenite, is partly included by orthopyroxene in the left portion and contacts directly with plagioclase in the right portion. Gabbroic inclusion 1C. Width is about 2870 μm.

Fig. 1-4. Enlarged image of Fig. 1-3. An intergrowth of magnesian orthopyroxene and whitlockite (Opx-Wht) occurs in close association with relic olivine. Small kamacite grains are sometimes observed in the Opx-Wht intergrowth. Gabbroic inclusion 1C. Width is about 395 μm.

Fig. 1-5. A relic olivine grain is included in a large orthopyroxene grain, and a large chromite grain is observed in the central portion. Gabbroic inclusion 1I. Width is about 2870 μm.

Fig. 1-6. Enlarged image of Fig. 1-5. Symplectic intergrowths of chromite and magnesian orthopyroxene (Sym), magnesian orthopyroxene (mOpx), whitlockite (Wht), and small kamacite (white) occur in close association with a relic olivine. Gabbroic inclusion 1I. Width is about 118 μm.

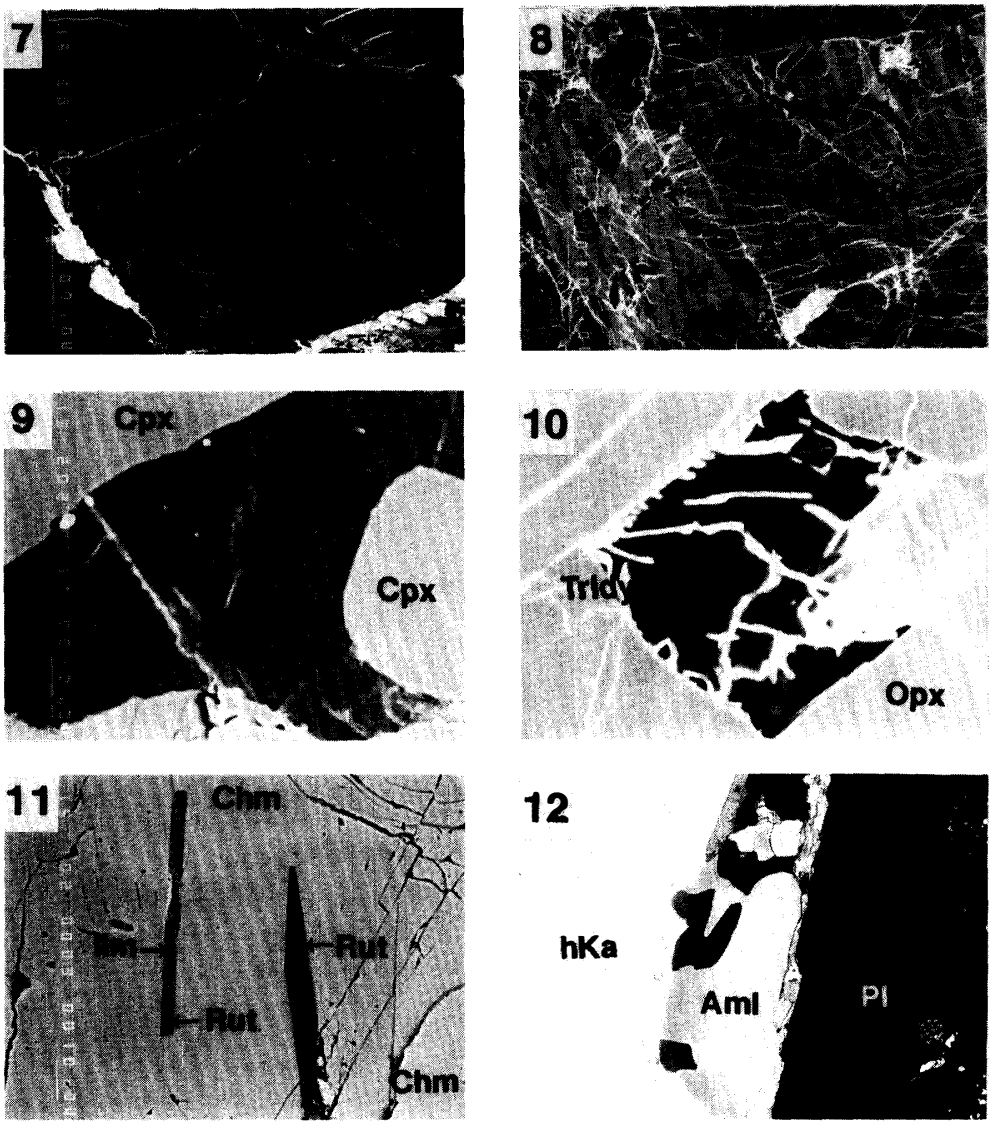

Fig. 1-7. Inverted pigeonite (IPig) consists of orthopyroxene host (dark) and clinopyroxene lamellae (light), and is partly included by clinopyroxene with narrow orthopyroxene lamellae. Gabbroic inclusion 2H. Width is about 395 μm.

Fig. 1-8. A large K-feldspar grain occurs in close association with intergrowths of anti-perthite (Ant-P) and tridymite. The anti-perthite consists of albite and K-feldspar lamellae, but the widths of the lamellae are variable. Gabbroic inclusion 2C. Width is about 395 μm.

Fig. 1-9. An intergrowth of albite and tridymite (Ab-Tridy) is rarely observed in interstitial spaces between pyroxene grains. Gabbroic inclusion 2D. Width is about 58 μm.

Fig. 1-10. Glass with rhyolitic composition rarely occurs in interstitial spaces between pyroxene grains. Small tridymite grains are observed in the glass. Gabbroic inclusion 2A. Width is about 58 μm.

Fig. 1-11. A large chromite, at the center of Fig. 1-5, includes lamellae of ilmenite and rutile in the core. Gabbroic inclusion 1I. Width is about 118 μm.

Fig. 1-12. Armalcolite occurs at a rim of gabbroic inclusion 1F. Width is about 395 μm.

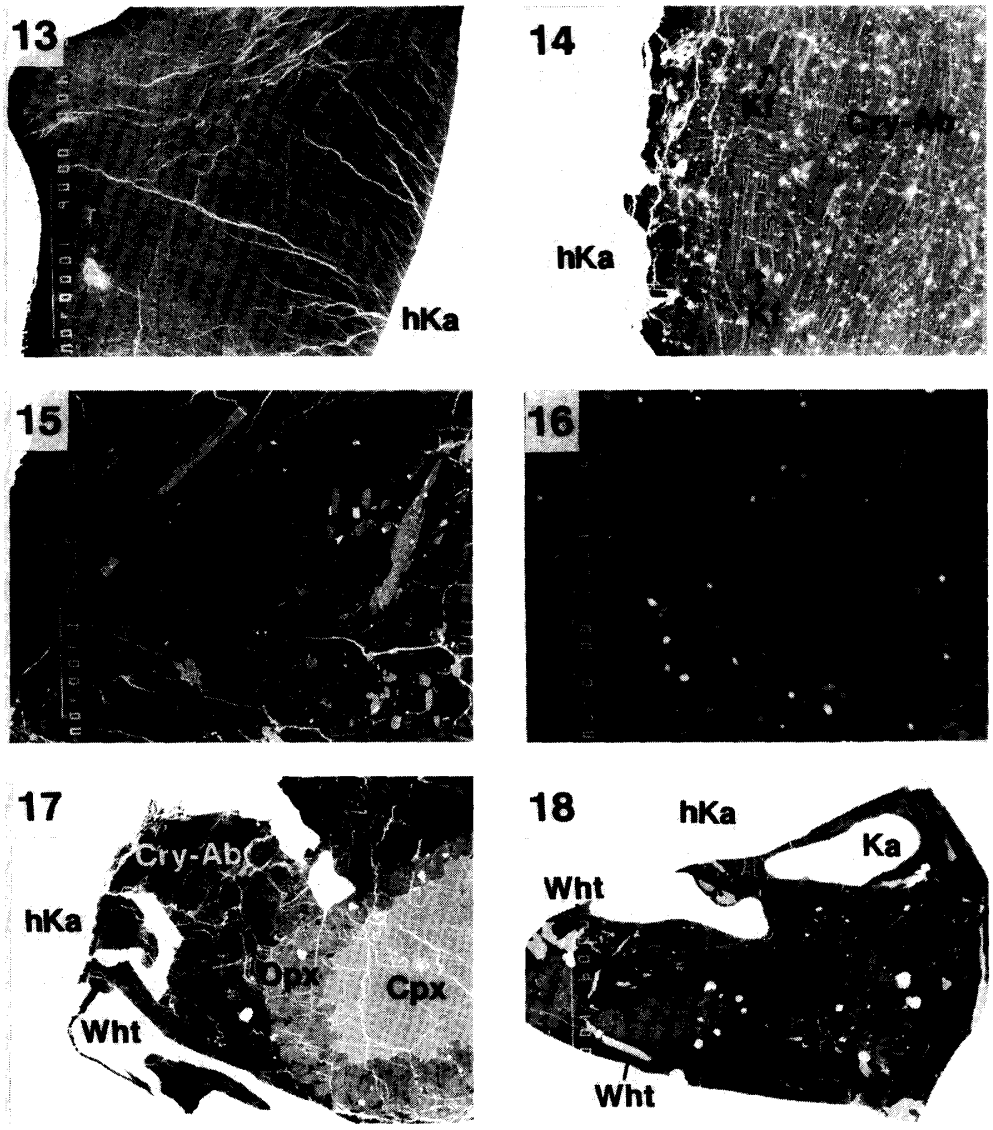

Fig. 1-13. Cryptocrystalline inclusion 1A. This inclusion appears to be massive and free of pyroxene phenocrysts. Width is about 2870 μm.

Fig. 1-14. Enlarged image of Fig. 1-13. Narrow K-feldspar streaks are common, and tiny kamacite grains (most are now altered to limonite) are scattered throughout the inclusion. Cryptocrystalline inclusion 1A. Width is about 435 μm.

Fig. 1-15. Alkali feldspar occurs as microphenocrysts, and the groundmass is cryptocrystalline albite. The microphenocrysts often show zoning from K-poor cores to K-rich rims. Laths of magnesian orthopyroxene (mOpx) occur in both microphenocrysts and the groundmass. Cryptocrystalline inclusion 1E. Width is about 395 μm.

Fig. 1-16. Cryptocrystalline inclusion 2E comprises many small bubbles and tiny kamacite grains (white spots, smaller than one micrometer) in addition to K-feldspar streaks. Width is about 39 μm.

Fig. 1-17. Cryptocrystalline inclusion 1G includes a large pyroxene phenocryst with a Cpx core and an Opx mantle. In addition, the inclusion comprises many microphenocrysts of alkali feldspar, and the groundmass is cryptocrystalline albite. Width is about 2870 μm.

Fig. 1-18. Cryptocrystalline inclusion 1H consists mainly of kamacite "baloons" orthopyroxene phenocrysts, whitlockite needles, small chromite grians, and cryptocrystalline albite groundmass. Width is about 2870 μm.

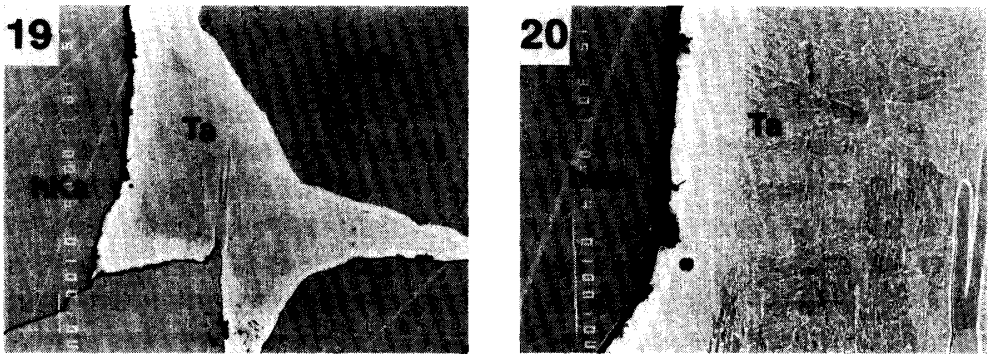

Fig. 1-19. The Miles host metal is almost all kamacite (hKa), but irregular taenite grains (Ta) are rarely observed. The taenite always shows zoning from Ni-poor cores to Ni-rich rims. Width is about 1180 μm.

Fig. 1-20. Enlarged image of Fig. 1-19. Note that the rim of taenite is rich in Ni (brighter) and that the core consists of a plessitic intergrowth of taenite and kamacite. Width is about 395 μm.

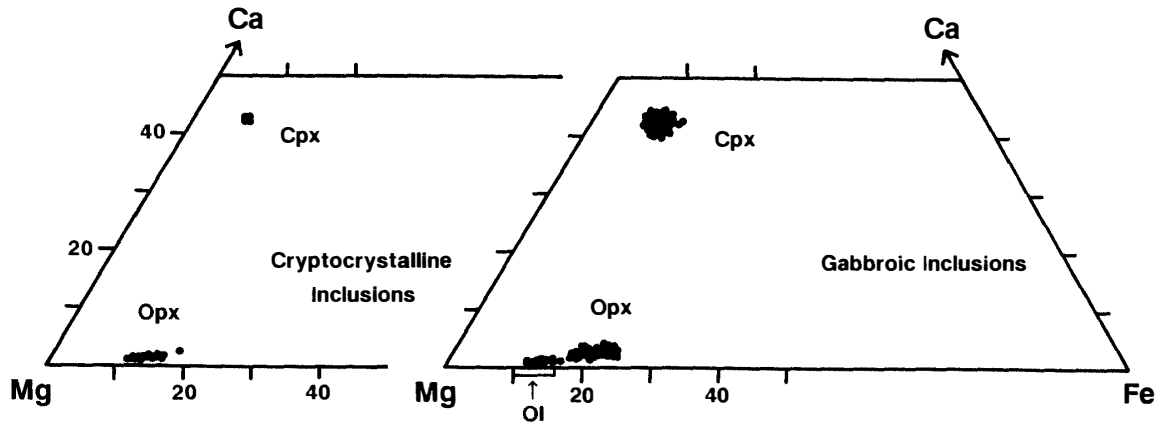

Fig. 2. Pyroxenes in gabbroic (right) and cryptocrystalline (left) inclusions from Miles are plotted in Ca-Mg-Fe atomic diagrams. The compositional range of relic olivines (Ol) in gabbroic inclusions are shown for reference. Most orthopyroxenes occurring as phenocrysts in gabbroic inclusions have mg ratios of 0.74 to 0.83, although orthopyroxenes occurring in close association with relic olivines are more magnesian than the phenocrystic orthopyroxenes. Orthopyroxene needles in cryptocrystalline inclusions have a compositional range similar to the magnesian orthopyroxenes in gabbroic inclusions.

these needles may be exsolution products. In addition to these occurrences, rutile and ilmenite occur as small grains independent of chromite, although ilmenite tends to occur in close association with olivine. Armalcolite is a rare mineral and occurs at the rims of some gabbroic inclusions (Fig. 1-12).

Both chlorapatite and whitlockite occur commonly at the rims of gabbroic inclusions (Fig. 1-1), and apatite is more abundant than whitlockite in gabbroic inclusions.

Metal in gabbroic inclusions is similar in chemical composition to the host metal (Fig. 6). However, metal occurring in close association with olivine shows a wider compositional range. Metal compositions of such occurrence in gabbroic inclusion 1C (Fig. 1-3) is plotted in a Ni-Co diagram (Fig. 6). Some kamacite grains included in a rutile grain are Ni-poor kamacite, with 1 wt% Ni, and some kamacites have high Co

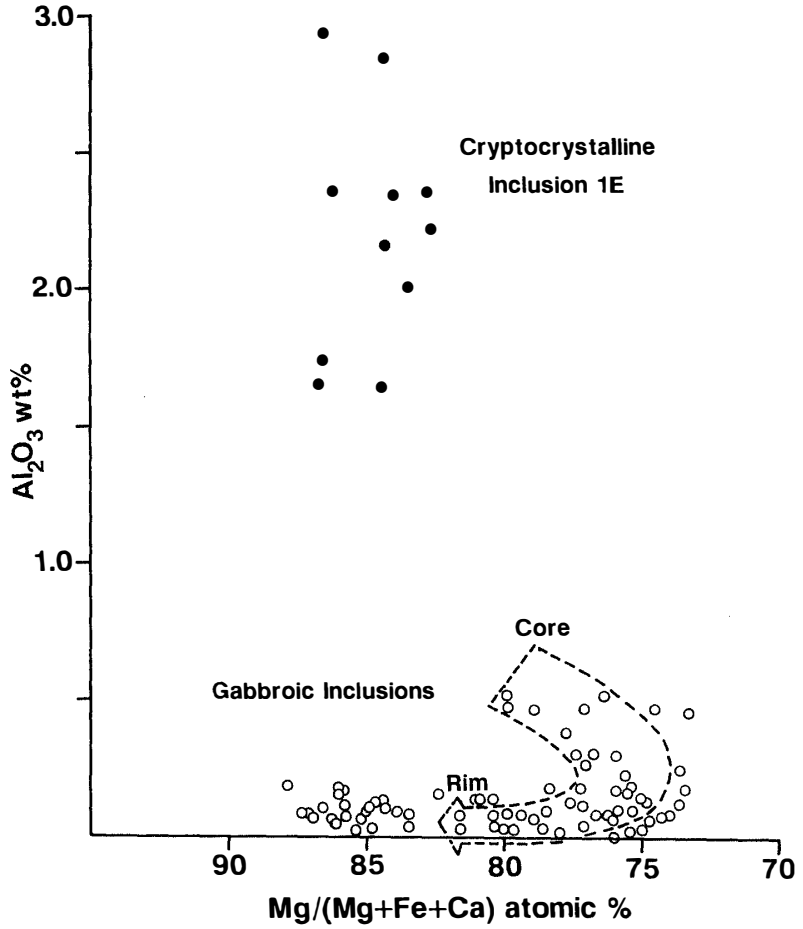

Fig. 3. Al_2O_3 contents of orthopyroxenes in gabbroic inclusions (open circles) and orthopyroxene needles in cryptocrystalline inclusions (solid circles) in Miles. The compositional range shown by the dashed lines was obtained from a large zoned orthopyroxene grain in a gabbroic inclusion (Fig. 5 in IKEDA and PRINZ, 1996), and show a trend from an Al-rich core to a magnesian Al-poor rim.

contents up to about 1.2 wt%, as shown in Fig. 6. The Ni-poor kamacite may have been produced by reduction of silicates, and the high Co contents of some metal may have been supplied from the breakdown of olivine (see later discussion). Schreibersite occurs in the peripheral portion of some gabbroic inclusions

3.3. Cryptocrystalline inclusions

Miles cryptocrystalline inclusions are massive (Fig. 1-13), include microphenocrysts of alkali feldspar (or anorthoclase) (Fig. 1-15, 1-17), or contain large pyroxene phenocrysts (Fig. 1-17, 1-18). High-Ca pyroxene phenocrysts in some cryptocrystalline inclusions sometimes have an orthopyroxene mantle (Fig. 1-17). The large pyroxene phenocrysts have a compositional range similar to those in gabbroic inclusions (Fig. 2), and may have been derived from the same reservoir as the gabbroic inclusions.

Some cryptocrystalline inclusions have microphenocrysts of alkali feldspar (Fig.

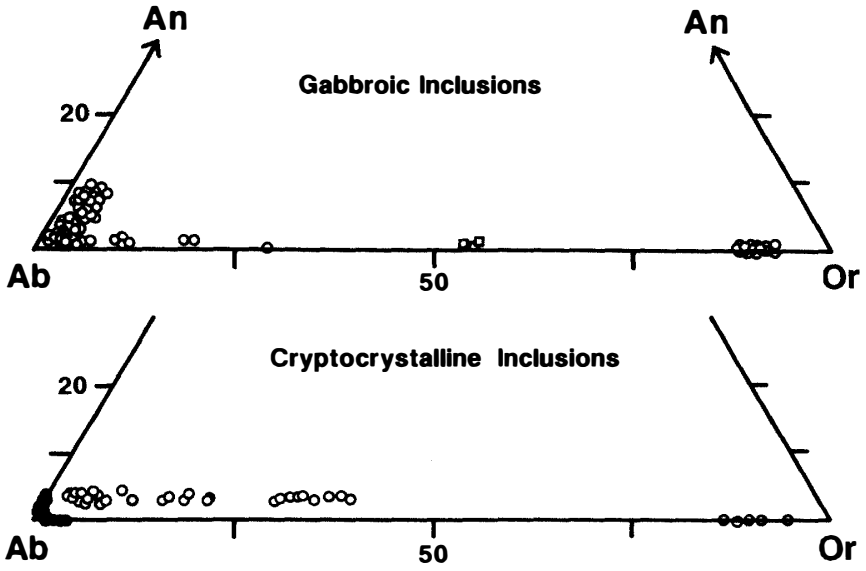

Fig. 4. Feldspars (open circles) and cryptocrystalline albite (solid circles) in gabbroic (upper) and cryptocrystalline (lower) inclusions from Miles are plotted in Ca (An, anorthite)-Na (Ab, albite)-K (Or, orthoclase) diagrams. In cryptocrystalline inclusions, microphenocrysts of alkali feldspar (open circles) occur in the groundmassic cryptocrystalline albite (solid circles). Glass with rhyolitic compositions, in gabbroic inclusion 2A, is shown for reference (square).

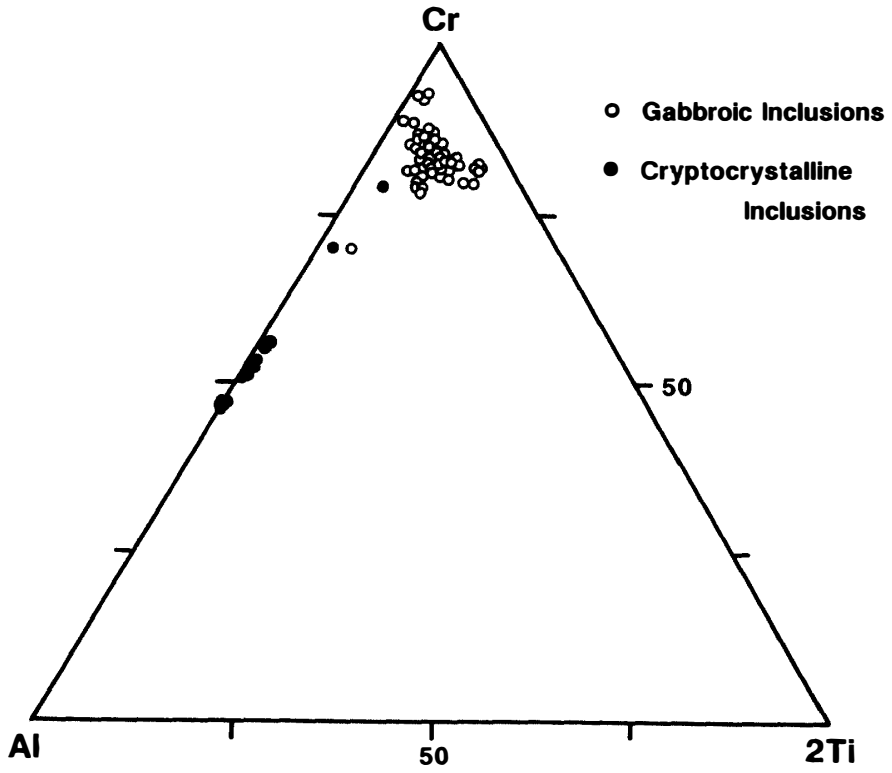

Fig. 5. Chromites in gabbroic (open circles) and cryptocrystalline (solid circles) inclusions are plotted in a Cr-Al-2Ti atomic diagram. Note that chromites in inclusion 1E, plotted around the Cr/(Cr + Al) ratio of 0.5, are aluminous in comparison to those in gabbroic inclusions.

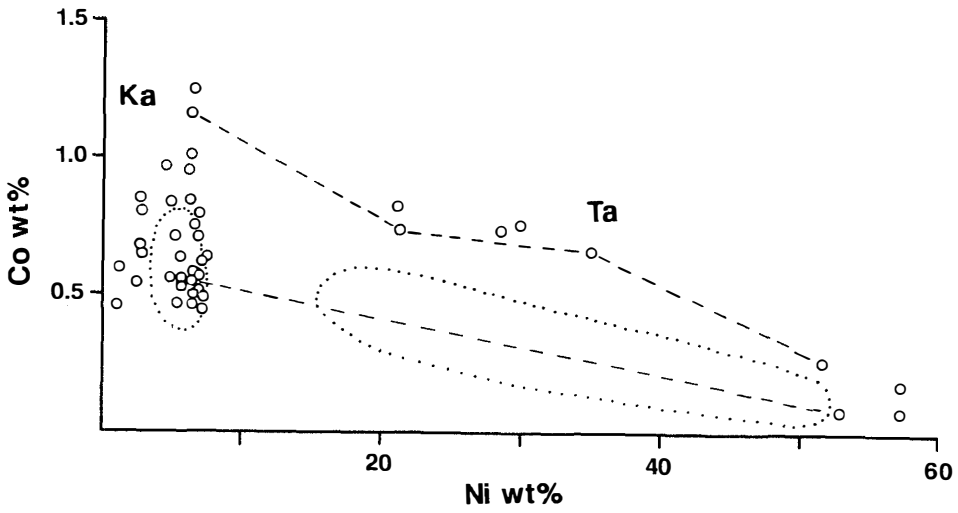

Fig. 6. Kamacite (Ka) and taenite (Ta) grains occurring in close association with relic olivine in gabbroic inclusion 1C (Fig. 1-3) are plotted in a Co-Ni diagram, in wt%. Kamacite and taenite which occur in the same grain are connected by dashed lines. The compositional ranges of kamacites and taenites occurring as host metal are shown by dotted lines. Metal occurring in close association with relic olivine has a wider compositional range than that in gabbroic inclusions free of relic olivine, which is similar in compositional range to that of the Miles host metal.

1-15, 1-17), which have zoning from K-poor cores to K-rich rims (Fig. 1-15). The compositions of the alkali feldspars range from Or_2 to Or_{40}, with constant An_{2-5} (Fig. 4). They seem to have crystallized *in situ*. In addition, needles of magnesian orthopyroxene (Fig. 1-15) occur in some inclusions, and their compositions are more magnesian than the phenocrystic orthopyroxene in gabbroic inclusions (Fig. 2). They have mg ratios from 0.88 to 0.80, with low Wo contents of 0.5 to 1.5% and are very similar to those occurring in close association with olivine in gabbroic inclusions (Fig. 2). However, the two magnesian orthopyroxenes differ in Al_2O_3 contents, as shown in Fig. 3; the magnesian orthopyroxene in cryptocrystalline inclusions contains high Al_2O_3, up to 3 wt%, whereas most of the magnesian orthopyroxene in gabbroic inclusions contains less than 0.2 wt%.

The groundmasses of cryptocrystalline inclusions are cryptocrystalline albite, and include K-feldspar streaks (Fig. 1-14), tiny kamacite grains (Fig. 1-14, 1-16), and small bubbles (Fig. 1-16). The composition of cryptocrystalline albites differ among the inclusions, and the range is shown in Fig. 4. The compositions of cryptocrystalline albites in inclusions 1E and 1G, which contain microphenocrysts of alkali feldspar, are An_{1-4}. However, other inclusions have cryptocrystalline albite which is free from An; their CaO contents are nearly zero.

Euhedral to subhedral chromite occurs commonly in cryptocrystalline inclusions, and is richer in Al than those in gabbroic inclusions (Fig. 5). In addition, chromite in cryptocrystalline inclusions is enriched in ZnO, ranging from 1.5 wt% (IKEDA and PRINZ, 1996) up to more than 4 wt% (Table 3).

Phosphate is very common in the cryptocrystalline inclusions, and whitlockite is more abundant than chlorapatite, in contrast to the more abundant occurrence of chlo-

rapatite in the gabbroic inclusions. Whitlockite-predominant nodules, reported in IKEDA and PRINZ (1996), were not observed in the cryptocrystalline inclusions studied here.

3.4. Host metal

The host metal of Miles is mainly kamacite and is free of Widmanstätten structure. Instead, irregular-shaped grains of taenite are rarely found in the host kamacite (Fig. 1-19), and it is zoned from Ni-poor cores (about 20 wt%) cores to Ni-rich rims (about 50 wt%) rims (Fig. 1-20). The Ni-poor cores form plessitic intergrowths of taenite and kamacite (Fig. 1-20), suggesting that the Miles iron formed under moderately-rapid cooling conditions at low temperatures. Schreibersite occurs commonly surrounding silicate inclusions and rarely in the host metal.

4. Discussion

4.1. Reduction by phosphorus

IKEDA and PRINZ (1996) found that phenocrystic orthopyroxenes in the Miles gabbroic inclusions show reverse zoning in the rims. They suggested that the reverse zoning was produced by reduction of the coexisting silicate melts and the reagent was phosphorus, supplied from the surrounding Fe-Ni-S-P melt into the silicate melts which crystallized the gabbroic inclusions. Here, we discuss the reduction by phosphorus, in more detail.

The gabbroic inclusions experienced reduction during their crystallization, and the reaction equation is;

$$\underset{\text{Silicate-melt}}{5FeO} + \underset{\text{Fe-melt}}{3CaO} + 2P \rightarrow \underset{\text{Metal}}{5Fe} + \underset{\text{Wht or Apt}}{Ca_3(PO_4)_2}, \quad (1)$$

where FeO and CaO in the reactants are components of the silicate melt, P is supplied from the surrounding Fe-Ni-S-P melt, and the products precipitate as metal, whitlockite (Wht), or chlorapatite (Apt). Reaction (1) may have decreased the FeO content of the silicate melts and they thus crystallized more magnesian and Ca-poor pyroxene. The reverse zoning of phenocrystic orthopyroxene in the gabbroic inclusions (Fig. 3) may be the result of the reduction of eq. (1). In addition, magnesian orthopyroxenes occurring in close association with olivine in some gabbroic inclusions have compositions which are on the extension of the reversely zoned orthopyroxene (Fig. 3). Therefore, these magnesian orthopyroxenes may also have been produced by the reduction by phosphorus.

HARLOW *et al.* (1980) discussed the solid state reduction in mesosiderites by using an equation ($5FeSiO_3 + 3CaSiO_3 + 2P \rightarrow 5Fe + Ca_3(PO_4)_2 + 8SiO_2$) which is similar to eq. (1). They found that phosphorus can be a reducing agent to produce magnesian orthopyroxene and that the temperature and oxygen fugacity are 1000°C and 10^{-17} atm for orthopyroxene of Fs_{60} and metal which includes 2 wt% P, and 770°C and 10^{-21} atm for Fs_{30} and metal with 0.03 wt% P. The reduction reaction of HARLOW *et al.* (1980) differs from eq. (1) in that the reactants of eq. (1) are components in silicate and metal liquids, and thus it is difficult to obtain the temperature-oxygen fugacity relations for eq. (1). However, the oxygen fugacity for Miles silicate inclusions may

have been nearly equal to or slightly lower than 10^{-17} atm at least in the latest stage of crystallization (solidus conditions, T=about 1000°C), because the orthopyroxene with $Fs_{15\text{-}20}$ (Fig. 3) coexists with high-Ca pyroxene, metal, whitlockite, and silica minerals in some gabbroic inclusions. The reversely zoned orthopyroxene may not have been produced by solid state reactions, because the inclusions contain glass and experienced rapid cooling under subsolidus condition. This is consistent with the facts that Miles sometimes includes sodalite or magnesian olivine together with silica minerals, and that chromite differs in composition among the silicate inclusions (IKEDA and PRINZ, 1996), indicating that the silicates were metastable under subsolidus conditions.

In Fig. 7, the MnO contents of minerals in the silicate inclusions are plotted against their FeO contents. The orthopyroxene and chromite in the cryptocrystalline inclusions are enriched in MnO in comparison to those in the gabbroic inclusions, indicating that they experienced reduction to a greater extent than the gabbroic inclusions. This is consistent with the fact that phosphates are more abundant in the cryptocrystalline inclusions. In addition, eq. (1) is consistent with the occurrence of most

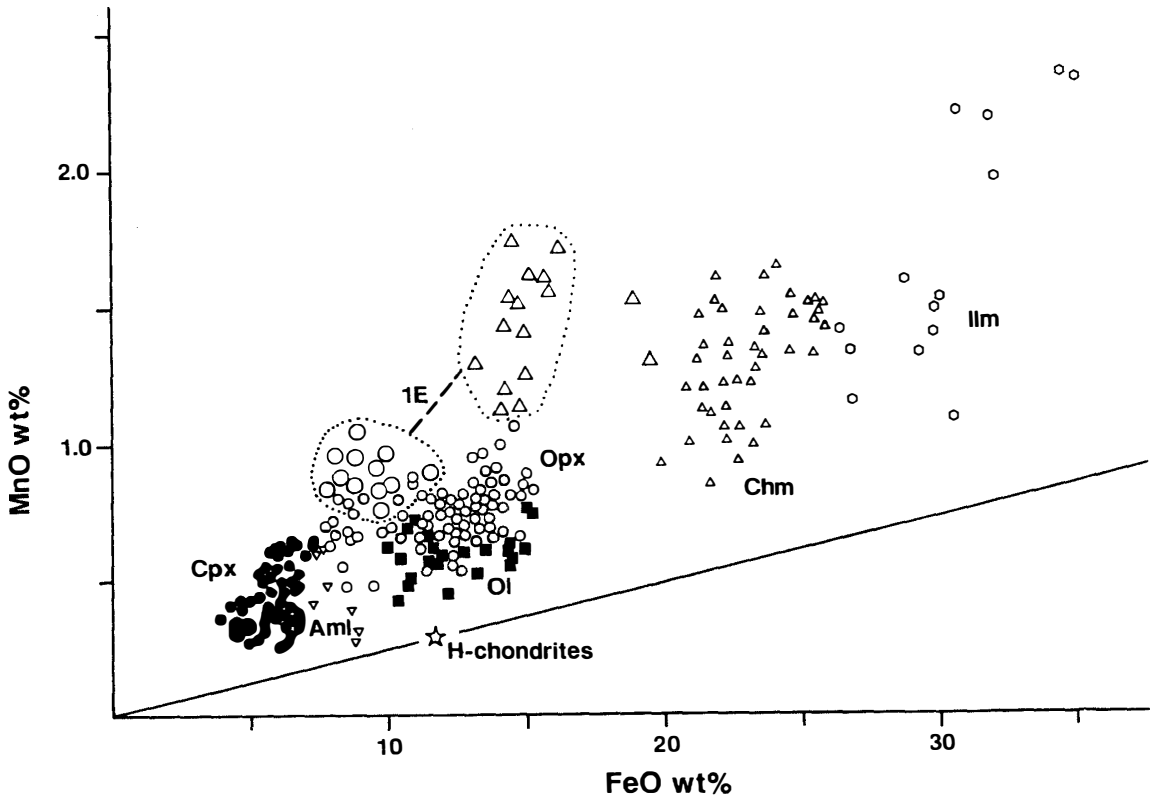

Fig. 7. MnO contents in high-Ca clinopyroxene (Cpx, solid circles), orthopyroxene (Opx, small open circles), olivine (Ol, solid squares), chromite (Chm, small open triangles), ilmenite (Ilm, open hexagons), and armalcolite (Aml, open reverse triangles) in gabbroic inclusions are plotted against their FeO contents. Orthopyroxenes (large open circles) and chromite (large open triangles) in cryptocrystalline inclusion 1E are also plotted together with a few chromites in other cryptocrystalline inclusions (large open triangles). An open star is average H-group chondrite (HARAMURA et al., 1983). Note that MnO/FeO ratios of the constituent minerals in Miles silicate inclusions are larger than that of average H-group chondrite.

phosphates being commonly located at the rims of the silicate inclusions (Figs. 1-1, 1-17, 1-18).

The cryptocrystalline albites in some inclusions are extremely depleted in CaO and thus free of An component. This depletion of CaO may be explained by reaction (1). In this case, anorthite components in the silicate melts are decomposed by the extraction of CaO to form phosphates, resulting in the enrichment of Al_2O_3 in the silicate melts. This enrichment of Al_2O_3 may explain the fact that chromites in the cryptocrystalline inclusions are more aluminous than those in the gabbroic inclusions. Plagioclase in the gabbroic inclusions is more depleted in anorthite component, on the whole, in comparison to that in equilibrated H-group chondrites (IKEDA and PRINZ, 1996), and this depletion may also be explained by eq. (1).

4.2. Olivine and the reaction zone

The Miles gabbroic inclusions have an average composition which plots near the liquidus field boundary between the olivine and low-Ca pyroxene fields in the fundamental basalt tetrahedron of the forsterite-diopside-albite-silica system (IKEDA and PRINZ, 1996). Therefore, olivine in some gabbroic inclusions might have been a primary liquidus phase which crystallized prior to low-Ca pyroxene, and later reacted with the silicate melt to produce low-Ca pyroxene. An alternative hypothesis for the origin of the olivine is that it is a relic mineral derived from the olivine-orthopyroxene residue which was produced by the partial or shock melting of H-group chondrites (IKEDA and PRINZ, 1996). It is difficult to determine which hypothesis is correct, except to say that olivine was not stable in the later stages of the crystallization of the Miles silicate melts.

The olivines are sometimes surrounded by a reaction zone which consists mainly of magnesian orthopyroxene, whitlockite, and metal, with intergrowths of magnesian orthopyroxene and whitlockite (Fig. 1-4) or symplectic intergrowths of magnesian orthopyroxene and chromite (Fig. 1-6). The reaction zone may be produced by the following equation;

$$\underset{\text{Ol}}{Mg_2SiO_4} + \underset{\text{Silicate-melt}}{3CaO + 5FeO} + \underset{\text{Fe-melt}}{2P} \rightarrow \underset{\text{mOpx}}{MgSiO_3} + \underset{\text{Wht}}{Ca_3(PO_4)_2} + \underset{\text{Met}}{5Fe} + MgO, \qquad (2)$$

where CaO and FeO in the reactants are components of the silicate melts, P is supplied from the surrounding Fe-Ni-S-P melt, and mOpx is magnesian orthopyroxene. The MgO in the products may be used to form magnesian ilmenite or to produce magnesian orthopyroxene with the SiO_2 component of the silicate melt. The magnesian orthopyroxene and whitlockite in the products of eq. (2) may have produced the intergrowths of these two minerals.

The symplectic intergrowths of magnesian orthopyroxene and chromite may form by the following equation (TAKEDA *et al.*, 1994); $MgFeSiO_4 + Cr_2O_3 \rightarrow MgSiO_3 + FeCr_2O_4$, where Cr_2O_3 is a component of the silicate melt. This equation has no relation to the reduction by phosphorus, but the decomposition of olivine may be preferable to the nucleation and growth of the symplectic intergrowths.

4.3. Origin of the Miles IIE iron

Our scenario for the origin of the Miles IIE iron is schematically shown in Fig. 8, and consists of the following stages. (1) Since porous materials can be heated up to high temperatures by impact shock (STÖFFLER *et al.*, 1988), regolithic H-group chondrites were melted by shock events on their parent body. This produced a silicate melt and an Fe-Ni-S-P melt, leaving olivine-orthopyroxene residues behind (OLSEN and JAROSEWICH, 1971; WASSON and WANG, 1986; IKEDA and PRINZ, 1996). The degree of shock melting was about 25% (IKEDA and PRINZ, 1996). The Fe-Ni-S-P melt was produced from metallic, sulfide, and phosphorus components of H-group chondrites. Average H-group chondrite has a metal-sulfide component with Fe=15.8 wt%, Ni=1.7 wt%, FeS=5.45 wt%, and P=0.1 wt% (HARAMURA *et al.*, 1983), and thus a recalculated compositions of Fe=83.56%, Ni=7.38%, S=8.63% and P=0.43%. (2) The silicate melt crystallized high-Ca pyroxene, pigeonite followed by orthopyroxene and plagioclase, and resulted in a crystal mush consisting of abundant phenocrysts and minor residual melt. The Fe-Ni-S-P melt also experienced crystallization of Ir-rich metal (see the companion paper, EBIHARA *et al.*, 1997). (3) The crystal mush and the Fe-Ni-S-P melt mixed with one another and two kinds of silicate melt inclusions were produced. One had a concentration of phenocrysts, with minor residual melt, resulting in silicate inclusions with irregular outlines. The other consisted mainly of residual silicate melts, with rare phenocrysts of pyroxene, resulting in silicate inclusions

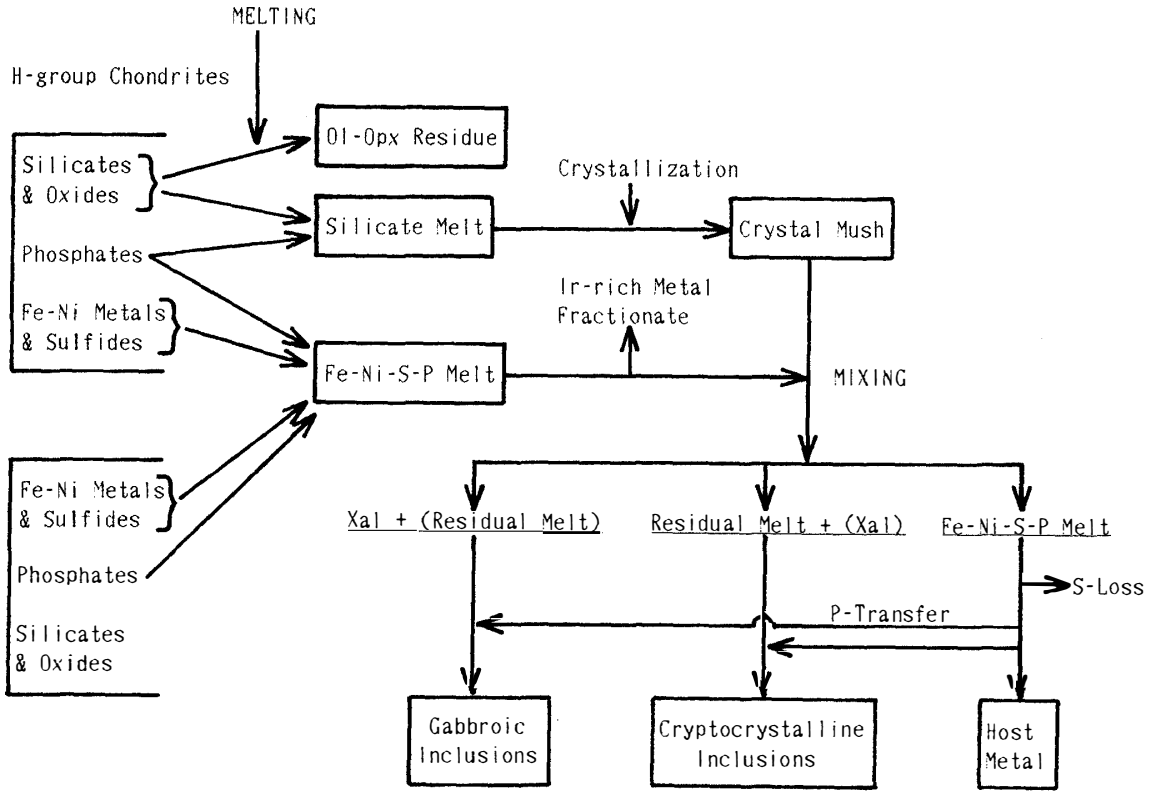

Fig. 8. Schematic diagram showing the origin of the Miles IIE iron (see text).

with round or ellipsoidal outlines. The latter melt inclusions were enriched in volatile components such as ZnO. (4) Most of the sulfur content of the Fe-Ni-S-P melt may have escaped to space (IKEDA and PRINZ, 1996), and this accelerated the crystallization of this melt. (5) Phosphorus in the Fe-Ni-S-P melt reacted with the silicate melt inclusions, and reduced them. Probably half of the phosphorus may have been used for the reduction process. (6) The two kinds of silicate melt inclusions resulted in the gabbroic and cryptocrystalline inclusions, and the host Fe-Ni-S-P melt completed its crystallization. At a late stage of crystallization, they cooled rapidly in the surficial region of the parent body to form glass in some gabbroic inclusions and cryptocrystalline groundmass in cryptocrystalline inclusions. The needle orthopyroxenes in cryptocrystalline inclusions may have crystallized *in situ* under rapid cooling conditions (IKEDA and PRINZ, 1996). The pigeonite which crystallized in stage (2) was already inverted to orthopyroxene, with augite lamellae, prior to the rapid cooling of this stage. (7) The other half of the phosphorus in the solid host metal exsolved as schreibersite around the silicate inclusions, but Widmanstätten structure was not produced in the host metal.

Acknowledgments

We thank Prof. J. T. WASSON and Prof. H. TAKEDA for critical reviews of the manuscript. This study was partially supported by funds from JAPS grant, Japan-Korea Co-operative Study on Antarctic Meteorites (to Y. IKEDA), and from NASA grant NAGW 34-90 (to M. PRINZ).

References

BENCE, A. E. and ALBEE, A. L. (1968): Empirical correction factors for the electron microanalysis of silicates and oxides. J. Geol., **76**, 382–403.

CLAYTON, R. N., MAYEDA, T. K., OLSEN, E. J. and PRINZ, M. (1983): Oxygen isotope relationships in iron meteorites. Earth Planet. Sci. Lett., **65**, 229–232.

EBIHARA, M., IKEDA, Y. and PRINZ, M. (1997): Petrology and chemistry of the Miles IIE iron. II: Chemical characteristics of the Miles silicate inclusions. Antarct. Meteorite Res., **10**, 373–388.

HARAMURA, H., KUSHIRO, I. and YANAI, K. (1983): Chemical compositions of Antarctic meteorites I. Mem. Natl Inst. Polar Kes., Spec. Issue, **30**, 109–121.

HARLOW, G. E., DELANEY, J. S., NEHRU, C. E. and PRINZ, M. (1980): The origin of abundant tridymite and phosphate in mesosiderites: Feasibility of possible reactions, Meteoritics, **15**, 297–298.

IKEDA, Y. and PRINZ, M. (1996): Petrology of silicate inclusions in the Miles IIE iron. Proc. NIPR Symp. Antarct. Meteorites, **9**, 143–173.

MCCOY, T. J. (1995): Silicate-bearing IIE irons: Early mixing and differentiation in a core-mantle environment and shock resetting of ages. Meteoritics, **30**, 542–543.

OLSEN, E. and JAROSEWICH, E. (1971): Chondrules: First occurrence in an iron meteorite. Science, **174**, 583–585.

OLSEN, E., DAVIS, A., CLARKE, R. S., SCHULTZ, L., WEBER, H. W., CLAYTON, R., MAYEDA, T., JAROSEWICH, E., SYLVESTER, P., GROSSMAN, L., WANG, M. S., LIPSHUTZ, M. E., STEELE, I. M. and SCHWADE, J. (1994): Watson: A new link in the IIE iron chain. Meteoritics, **29**, 200–213.

PRINZ, M., NEHRU, C., DELANEY, J., WEISBERG, M. and OLSEN, E. (1983): Globular silicate inclusions in IIE irons and Sombrerete: Highly fractionated minimum melts. Lunar and Planetary Science XIV. Houston, Lunar Planet. Inst. 616–617.

RUBIN, A. E., JERDE, E., ZONG, P., WASSON, J. T., WESTCOTT, J. W., MAYEDA, T. K. and CLAYTON, R. N.

(1986): Properties of the Guin ungrouped iron meteorite: The origin of Guin and of group-IIE irons. Earth Planet. Sci. Lett., **76**, 209–226.

STÖFFLER, D., BISHOFF, A., BUCHWALD, V. and RUBIN, A. E. (1988): Shock effects in meteorites. Meteorites and The Early Solar System ed. by J. F. KERRIDGE and J. F. MATHEWS. Tucson, Univ. Arizona Press, 165–202.

TAKEDA, H., MORI, H., HIROI, T. and SAITO, J. (1994): Mineralogy of new Antarctic achondrites with affinity to Lodran and a model of their evolution in an asteroid. Meteoritics, **29**, 830–842.

WASSERBURG, G. J., SANZ, H. G. and BENCE, A.E. (1986): Potassium-feldspar phenocrysts in the surface of Colomera, and iron meteorite. Science, **161**, 684–687.

WASSON, J. T. and WANG, J. (1986): A nonmagmatic origin of group-IIE iron meteorites. Geochim. Cosmochim. Acta, **50**, 725–732.

(*Received August 27, 1996; Revised manuscript accepted December 9, 1996*)